

# Spectral Changes Induced by a Phase Modulator Acting as a Time Lens

## Introduction

First noted in the 1960s, a mathematical equivalence exists between paraxial-beam diffraction and dispersive pulse broadening.<sup>1,2</sup> This equivalence, known as space–time duality, has led to the development of temporal analogs of several spatial optical devices. An important component of such devices is the time lens,<sup>3,4</sup> which is designed to impose a time-dependent parabolic phase across an optical pulse passing through it, just as a traditional lens provides a parabolic phase in space. The development of such a time lens has led to applications such as temporal imaging,<sup>3–6</sup> spectral phase conjugation,<sup>6</sup> and temporal cloaking.<sup>6,7</sup>

Although modern time lenses typically produce the required parabolic phase using nonlinear effects such as four-wave mixing,<sup>6–9</sup> any device that provides a time-dependent parabolic phase can function as a time lens. By using an electro-optic effect to provide this phase, the pulse spectrum can be manipulated without the use of optical nonlinear effects such as self-phase modulation.

An electro-optic phase modulator driven by a sinusoidal signal approximates the parabolic phase of a time lens. This approximation holds for optical pulses aligned with a local maximum or minimum of the modulation cycle. Time lenses made with this arrangement have been well explored.<sup>6,10,11</sup> The behavior for nonstandard configurations, however, where a temporal offset exists between the modulator voltage and optical pulse, has attracted much less attention.

In this article it is shown that by changing this temporal offset, the spectrum of an optical pulse could be selectively broadened, narrowed, or frequency shifted without requiring optical nonlinearities. The following sections (1) present a relevant theory and show the results of numerical simulations; (2) verify theoretical predictions with an experiment performed using 4-ps pulses at 1053 nm and a lithium niobate phase modulator capable of providing a maximum phase shift of 16 rad at a 10-GHz modulation frequency; and (3) summarize the main results.

## Numeric Simulations and Theory

The Fourier-lens configuration, in which an input pulse first propagates inside a dispersive medium before passing through a time lens, is considered first. The length of dispersive medium in this configuration is chosen to be equal to the focal length of the lens. For a linear system, the electric field at the output of the dispersive medium can be related to the input electric field as

$$E_{\text{out}}(t) = \int_{-\infty}^{\infty} E_{\text{in}}(t')h(t-t')dt', \quad (1)$$

where  $h(t)$  is the impulse response of the linear dispersive medium of length  $L$  with the Fourier transform  $\exp[i\beta(\omega)L]$  and  $\beta(\omega)$  is the propagation constant inside the dispersive medium. If  $\phi_m(t)$  is the phase shift imposed by the modulator, the pulse spectrum is obtained by taking the Fourier transform as

$$\tilde{E}_{\text{out}}(\omega) = \int_{-\infty}^{\infty} E_{\text{out}}(t)\exp[i\phi_m(t)]e^{i\omega t} dt. \quad (2)$$

Using the convolution theorem in Eq. (1),  $E_{\text{out}}(t)$  is related to the Fourier transform of  $E_{\text{in}}(t)$  as

$$E_{\text{out}}(t) = \frac{1}{2\pi} \int_{-\infty}^{\infty} \tilde{E}_{\text{in}}(\omega)\exp[i\beta(\omega)L]d\omega. \quad (3)$$

In practice, the propagation constant  $\beta(\omega)$  is Taylor expanded around the central frequency  $\omega_0$  of the pulse spectrum as<sup>12</sup>

$$\beta(\omega)L = \beta_0L + \beta_1L(\omega - \omega_0) + \frac{1}{2}\beta_2L(\omega - \omega_0)^2 + \dots \quad (4)$$

Here,  $\beta_0L$  leads to a constant phase shift and  $\beta_1L$  is a constant temporal delay with no impact on the pulse shape or spectrum. In contrast,  $\beta_2L$  affects not only the width but also the chirp of the pulse.

When an electro-optic phase modulator driven by a sinusoidal clock signal is used as the time lens, the phase shift imposed by it has the form

$$\phi_m(t) = \phi_0 \cos(\omega_m t - \theta), \quad (5)$$

where  $\phi_0$  is the peak amplitude,  $\omega_m$  is the modulation frequency, and  $\theta = \omega_m t_0$  is the phase offset resulting from the time offset  $t_0$  between the peak of the sinusoidal voltage and the peak of the optical pulse. For  $\theta = 0$ , the peak of the sinusoid coincides with the peak of the optical pulse at  $t = 0$ .

In an analogy to the focal length of a traditional lens, the focal group-delay dispersion (GDD) is used to describe a time lens<sup>4</sup> through  $D_f = -1/(\phi_0 \omega_m^2)$ . In the Fourier-lens configuration, the length of the dispersive medium is chosen such that  $D_f = \beta_2 L$ .

To study the impact of finite values of  $\theta$ , the integral in Eq. (3) is calculated numerically and then obtained the spectrum of the output pulse as indicated in Eq. (2). The results presented in Fig. 142.22 show the pulse spectra as functions of  $\theta$  over one modulation cycle as a color-coded surface plot. The parameter values for numerical simulations were chosen to match the capabilities of a modern, commercially available LiNbO<sub>3</sub> phase modulator operating at  $\lambda_0 = 1053$  nm. More specifically,  $\omega_m/2\pi = 10$  GHz and  $\phi_0 = 30$  rad. These values

result in a time aperture of  $\Delta T = 1/\omega_m = 15.9$  ps and a temporal resolution of  $\delta t = 2.77/(\phi_0 \omega_m) = 1.47$  ps (Ref. 6). The focal GDD for the time lens is  $D_f = -8.44$  ps<sup>2</sup>. The temporal phase imparted by the time lens was included exactly using Eq. (5). The dispersion for these simulations is assumed to be ideal, and all coefficients beyond  $\beta_2$  in Eq. (4) are ignored.

Figure 142.22 shows the results for Gaussian input pulses of widths (a) 1.5 ps and (b) 20 ps, with spectral bandwidths of 1.08 nm and 81.4 pm, respectively (all full widths at half maximum). The spectral behavior is quite different for the two pulse widths. It is stressed that even though the pulse spectrum varies considerably with the angle  $\theta$ , the temporal shape of output pulses remains the same for all  $\theta$ .

Figure 142.22(a) obtained for 1.5-ps input pulses shows that the pulse spectrum is narrowest near  $\theta = 0$ . It begins to broaden and shift toward shorter wavelengths as  $\theta$  increases, and the maximum shift of about 1.32 nm occurs for  $\theta = \pi/2$ . After this value, the spectrum shifts toward longer wavelengths, and the spectral width continues to increase until  $\theta = \pi$ , where it reaches its maximum value of 2.23 nm. The spectrum continues to shift toward longer wavelengths until  $\theta$  reaches the value  $3\pi/2$ . Beyond this, the spectrum begins to narrow and recovers its original size at  $\theta = 2\pi$ . Note that the spectral evolution is antisymmetric with respect to  $\theta = \pi$ .

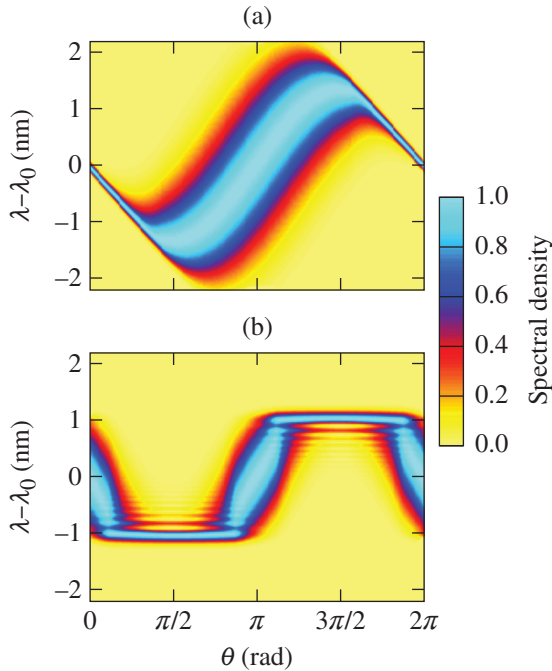
To understand the physical origin of these spectral changes, it is useful to expand  $\phi_m(t)$  in Eq. (5) as a Taylor series around  $t = 0$  as

$$\phi_m(t) = \phi_0 \left\{ \cos\theta - (\omega_m \sin\theta)t - \left[ \frac{\omega_m^2}{2} \cos(\theta) \right] t^2 + \dots \right\}. \quad (6)$$

When there is no phase offset ( $\theta = 0$ ), all odd-order terms vanish in the Taylor expansion. If terms only up to the second order are retained,

$$\phi_m(t) = \phi_0 \left( 1 - \omega_m^2 t^2 / 2 \right). \quad (7)$$

The quadratic term provides a time-dependent parabolic phase shift and fulfills the function of an ideal time lens. The higher-order phase terms in Eq. (6) lead to the temporal equivalent of spatial aberrations and cause distortions in the output pulse shape and spectrum. The time aperture, as defined earlier, is the temporal range over which these higher-order phase terms are small and do not noticeably distort the output of the time lens.<sup>4</sup>



E23823JR

Figure 142.22 Surface plots showing simulated output spectra for different values of  $\theta$  when (a) 1.5-ps and (b) 20-ps Gaussian pulses are sent through a phase modulator acting as a time lens. The color bars show the range of spectral density, normalized to 1 at its peak for each value of  $\theta$ .

The features seen in Fig. 142.22(a) can be understood from Eqs. (2) and (6). It is easy to see that the linear term in the Taylor expansion in Eq. (6) corresponds to a frequency shift in the pulse spectrum by an amount

$$\Delta\omega = \phi_0(\omega_m \sin\theta). \quad (8)$$

This shift is maximum when  $\theta = \pi/2$  and has the value  $\Delta\nu = \phi_0\omega_m/2\pi$ . For values of  $\phi_0 = 30$  rad and  $\omega_m/2\pi = 10$  GHz, this gives a maximum shift of 300 GHz or 1.11 nm at  $\lambda = 1053$  nm—a value that is close but not identical to the numerical value of 1.32 nm in Fig. 142.22(a). The source of this difference will be discussed later. It is important to note that the frequency shift is the same regardless of the central wavelength of the input pulse. Therefore, a phase modulator with the same parameters operating at a longer wavelength would produce a larger wavelength shift. For example, a phase modulator at 1550 nm with the same parameters would produce a wavelength shift of about 2.4 nm.

In addition to the linear phase term, the parabolic phase term changes with  $\theta$  as  $\phi_2 = -\phi_0\omega_m^2 \cos(\theta)$ . This dependence changes the focal GDD of the time lens as  $D_f(\theta) = -[\phi_0\omega_m^2 \cos(\theta)]^{-1}$ . The minimum focal GDD occurs at  $\theta = 0$  and increases in magnitude for other phase offsets. Additionally, the sign of the focal GDD is inverted between  $\theta = \pi/2$  and  $\theta = 3\pi/2$ . This situation is analogous to changing from a convex to a concave lens. Changes in the bandwidth of the output spectrum seen in Fig. 142.22(a) result from this  $\theta$  dependence of the focal GDD.

Figure 142.23 compares the output and input spectra of 1.5-ps pulses for three specific values of  $\theta$ . In Fig. 142.23(a), the

width of the output spectrum is only 0.136 nm, i.e., the output spectrum is narrowed by a factor of nearly 8 when compared to the input spectrum. This spectral compression is the temporal analog of the collimation of an optical beam realized with a lens and may be useful for applications requiring a narrow-bandwidth source. Just as in the spatial case, where angular divergence is reduced by expanding the size of the optical beam, spectral compression is accomplished at the expense of a broader pulse. The dispersive medium broadens the pulse while chirping it simultaneously, and the modulator is used to cancel the chirp and produce a transform-limited pulse. For this reason, the spectrum is compressed by the same factor by which the pulse broadens in the time domain.

Figure 142.23(b), drawn for  $\theta = \pi/2$ , shows that the spectrum is shifted toward shorter wavelengths by 1.32 nm without a significant change in the spectral width. Such wavelength shifts do not require the Fourier-lens configuration and have been used for spectral shearing interferometry by passing a pulse directly through a modulator.<sup>13</sup> In our case, the spectral shift reaches a maximum at  $\theta = \pi/2$  and  $\theta = 3\pi/2$  as predicted by the theory, where the peak of the pulse coincides with the maximum slope of the time-dependent phase. Deformation of the spectral shape in Fig. 142.23(b) is caused by the cubic term in Eq. (6). This term is also responsible for the larger 1.32-nm shift compared to that predicted by the linear term. Indeed, if the simulations are repeated and only kept up to the quadratic terms of Eq. (6), the input and output spectra become identical except for a spectral shift whose magnitude of 1.11 nm coincides with the theoretical estimate presented earlier.

Figure 142.23(c) shows that the spectral shift disappears for  $\theta = \pi$ . This feature is easily understood from Eq. (6), showing

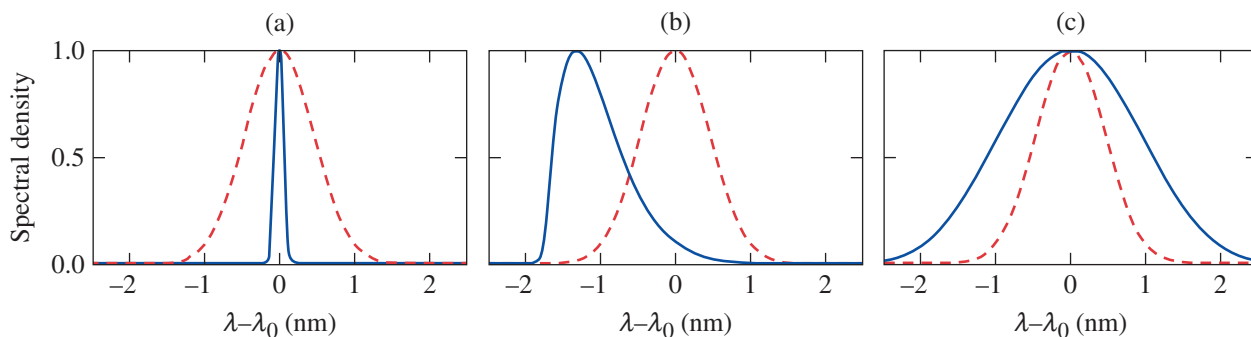


Figure 142.23

Comparison of input (dashed) and output (solid) spectra for a 1.5-ps input pulse at clock phases (a)  $\theta = 0$ , (b)  $\theta = \pi/2$ , and (c)  $\theta = \pi$ .

that both the linear and cubic terms vanish for this value of  $\theta$ . Finally, the spectral broadening seen in Fig. 142.23(c) originates from the sign change of the quadratic term in Eq. (6) for  $\theta = \pi$ . In effect, the modulator is now acting analogous to a concave lens that increases the angular spread of a beam incident on it.

The 2.23-nm spectral bandwidth, occurring at  $\theta = \pi$ , indicates broadening by a factor of about 2. Unlike spectral broadening from effects like self-phase modulation, the spectrum broadened by a time lens maintains its initial shape, as is apparent in Fig. 142.23(c). Slight distortions in the spectral wings have their origin in the fourth-order term in Eq. (6).

The results of Fig. 142.22(b) show that for the 20-ps input pulse, the pulse experiences negligible broadening when passing through the dispersive medium. However, the pulse is already longer than the aperture of the time lens. This results in a behavior that is qualitatively different from that seen in Fig. 142.22(a) for the shorter 1.5-ps pulse. More specifically, the spectrum is wider at  $\theta = 0$  and becomes narrowest at  $\theta = \pi/2$ , reaching a minimum bandwidth of 0.158 nm. The spectrum then broadens again near  $\theta = \pi$ , where the time lens once again acts like a concave lens and reaches a bandwidth of 1.58 nm. The behavior at  $\theta = 0$  and  $\theta = \pi$  is analogous to a highly collimated optical beam incident on either a convex lens or a concave lens, respectively. For a highly collimated beam, the beam shape does not change with propagation. The angular spread of the beam is affected, however, by the lens: both convex and concave lenses expand it.

## Experimental Results

A schematic of the experimental setup is shown in Fig. 142.24. A mode-locked laser<sup>14</sup> producing 150-fs pulses at 1053 nm, with a 38-MHz repetition rate, was used as a source of optical pulses. The time lens was implemented using an electro-optic phase modulator. A high-efficiency lithium niobate phase modulator<sup>15</sup> designed to operate at a wavelength of 800 nm but usable at 1053 nm was used. The 10-GHz clock signal used to drive the phase modulator was produced with phase locking.<sup>16</sup> A fast photodiode created an electronic signal of the laser pulse train, and a 76-MHz bandpass filter produced a synchronization signal at the second harmonic of the 38-MHz laser repetition rate. This 76-MHz signal matches the resonant frequency of a commercially available phase-locked dielectric resonator oscillator (PDRO), and it was locked to one of the harmonics of the 76-MHz signal around 10 GHz. The 10-GHz output was sent through a “trombone” phase shifter controlled with a translation stage driven by a stepper motor. Using an oscilloscope,

each step of the motor was found to produce a 42-fs delay in the 10-GHz clock signal, corresponding to 2.63 mrad of clock phase shift. The shifted signal was amplified by a 33-dBm microwave amplifier and used to drive the phase modulator. This setup produced a peak phase shift of  $\phi_0 = 16$  rad, a value lower than the 30 rad used in numerical simulations. For this reason, the range of spectral bandwidths and spectral shifts is reduced compared to the simulations. The time lens has a time aperture of  $\sim 15.9$  ps, a resolution time of  $\delta t = 2.8$  ps, and a focal GDD of  $D_f = -15.8$  ps<sup>2</sup>.

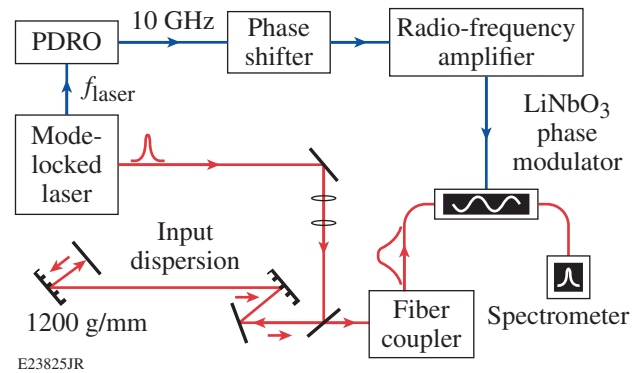


Figure 142.24

Experimental setup for a time-to-frequency converter using a phase modulator as a time lens. PDRO: phase-locked dielectric resonator oscillator.

The time lens was used in the Fourier-lens configuration, and a grating pair was used as a dispersive delay line. The delay line was created using two 1200-lines/mm reflective diffraction gratings separated by 80 cm with an incident angle of 25.3° to produce a GDD that matched  $D_f = -15.8$  ps<sup>2</sup> of our time lens. The chirped and broadened pulse was then sent through the phase modulator. For different clock phases, the pulse spectrum was recorded using an optical spectrum analyzer.<sup>17</sup>

Two different filters were applied to the laser signal to broaden the 150-fs pulses. A slit filter was used between the parallel gratings to create a spectral width of 0.407 nm, corresponding to Gaussian pulses of  $\sim 4$ -ps duration. In addition, a volume Bragg grating with a spectral width of 0.108 nm produced longer pulses of  $\sim 19$ -ps duration, assuming transform-limited pulses.

The experimentally recorded spectra are shown in Fig. 142.25. Comparing the short-pulse cases of Fig. 142.25(a) with Fig. 142.22(a), it is seen that the two cases agree qualita-

tively. In particular, the experimental spectra follow an identical progression as  $\theta$  advances through the phase-modulation cycle. As predicted by theory in the previous section, the experimental spectrum is narrowest at  $\theta = 0$ , reaches maximum spectral shift at  $\theta = \pi/2$  and  $\theta = 3\pi/2$ , and exhibits the largest spectral broadening at  $\theta = \pi$ .

Figure 142.26 compares [(a)–(c)] the experimentally recorded and [(d)–(f)] theoretically predicted output spectra for the same three values of  $\theta$  in the case of 4-ps input pulses. The numerical simulations used the experimentally recorded input spectrum (shown by a red dashed line for comparison) to obtain the temporal profile, assuming that pulses were transform limited. The agreement between the theory and experiment is quite good in all cases.

In agreement with the numerical simulations presented in the previous section, spectral compression at  $\theta = 0$  in Figs. 142.26(a) and 142.26(d) is observed. The width of the output spectrum is 0.18 nm, indicating that the pulse spectrum is compressed by a factor of about 2, which is considerably smaller than the factor of 8 observed in Fig. 142.23(a). The reduced compression factor is caused by the smaller spectral width of 4-ps input pulses and 16-rad maximum phase shift of the modulator used in our experiment. For the same reason, the spectral shift of 0.68 nm seen in Fig. 142.26(b) for  $\theta = \pi/2$  is also smaller compared to that seen in Fig. 142.23(b). The spectrum in Fig. 142.26(b) also has a small bump near  $\lambda = \lambda_0$  that is not present in Fig. 142.26(e). This bump arises from the polarization dependence of our phase modulator. More specifically, the modulator produces a significantly smaller

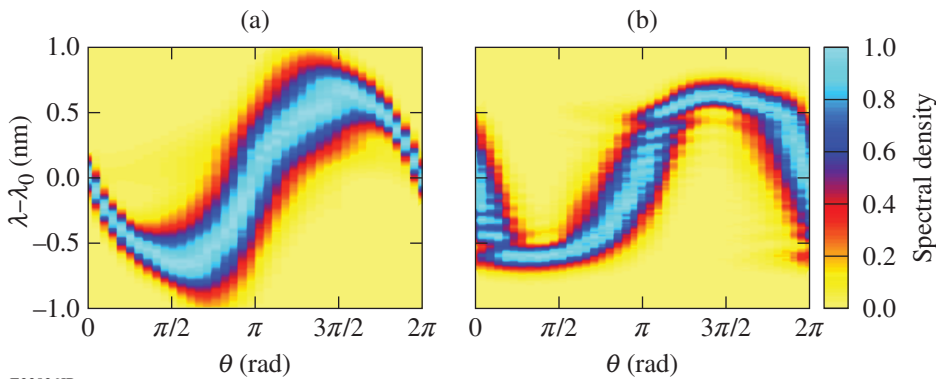


Figure 142.25

Surface plots showing experimental output spectra for different values of  $\theta$  when input pulses were filtered to produce (a) 0.407- and (b) 0.107-nm-wide input spectra. The color bars show the range of spectral density, normalized to 1 at its peak for each value of  $\theta$ .

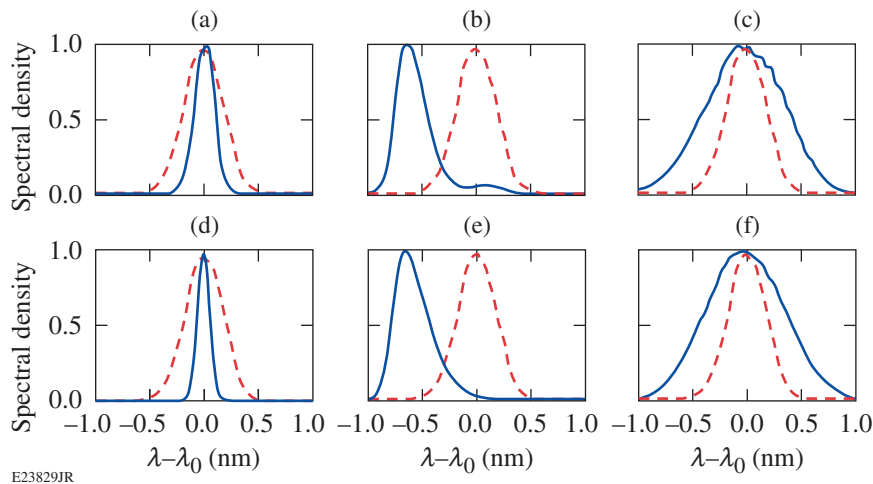


Figure 142.26

Comparison of [(a)–(c)] experimental and [(d)–(f)] simulated output spectra (solid blue line) for [(a),(d)]  $\theta = 0$ , [(b),(e)]  $\theta = \pi/2$ , and [(c),(f)]  $\theta = \pi$ . The input spectrum is shown by the dashed red line.

value of  $\phi_0$  along the slow axis compared to the fast axis. A small mismatch between the pulse's polarization direction and the slow axis of the phase modulator produces the bump in the spectrum seen in Fig. 142.26(b). Because our theory does not include polarization effects, this bump is not reproduced in Fig. 142.26(e).

As seen in Figs. 142.26(c) and 142.26(f), the pulse spectrum has a bandwidth of 0.86 nm when  $\theta = \pi$ , i.e., it has been broadened by a factor of 2.1, while the shape of the input spectrum is nearly preserved. Some distortion of the spectral shape is observed because the pulse is chirped in time during the input dispersion, causing wavelengths farther away from the central wavelength to move toward the wings of the pulse. Since pulse wings experience aberrations from higher-order phase terms in the time lens, small distortions appear in the shape of the spectrum. It is emphasized, however, that a suitably designed time lens can broaden considerably the spectrum of a pulse without significantly distorting its shape. In this respect, a time lens is superior to the use of self-phase modulation, which invariably distorts the spectrum while broadening it (and also requires high pulse energies).

### Conclusion

Spectral narrowing, broadening, and shifts have been demonstrated for picosecond pulses using a lithium niobate electro-optic phase modulator acting as a time lens. These spectral effects depend on the maximum phase shift that can be imposed by the modulator. In the numerical simulations presented, the pulse spectrum was compressed by a factor of 8 for a 30-rad phase shift. Experimentally, spectral shifts over a 1.35-nm range and spectral narrowing and broadening by a factor of 2 were demonstrated using a lithium niobate phase modulator with a maximum phase shift of 16 rad at a 10-GHz modulation frequency. More-dramatic narrowing, broadening, and shifts could be achieved by cascading multiple phase modulators to produce higher phase amplitudes and shorter focal GDD's. This work shows that a phase modulator can be used to tune the central frequency and the spectral bandwidth of picosecond pulses emitted by mode-locked lasers.

### ACKNOWLEDGMENT

B. Plansinis was supported by a Horton Fellowship. This material is based upon work supported by the Department of Energy National Nuclear Security Administration under Award Number DE-NA0001944, the University of Rochester, and the New York State Energy Research and Development Authority. The support of DOE does not constitute an endorsement by DOE of the views expressed in this article.

### REFERENCES

1. P. Tourniois, C. R. Acad. Sci. **258**, 3839 (1964).
2. S. A. Akhmanov, A. P. Sukhorukov, and A. S. Chirkin, Sov. Phys. JETP **28**, 748 (1969).
3. B. H. Kolner and M. Nazarathy, Opt. Lett. **14**, 630 (1989).
4. B. H. Kolner, IEEE J. Quantum Electron. **30**, 1951 (1994).
5. C. V. Bennett and B. Kolner, IEEE J. Quantum Electron. **36**, 430 (2000).
6. R. Salem, M. A. Foster, and A. L. Gaeta, Adv. Opt. Photon. **5**, 274 (2013).
7. M. Fridman *et al.*, Nature **481**, 62 (2012).
8. D. H. Broaddus *et al.*, Opt. Express **18**, 14,262 (2010).
9. A. Pasquazi *et al.*, IEEE J. Sel. Top. Quantum Electron. **18**, 629 (2012).
10. A. A. Godil, B. A. Auld, and D. M. Bloom, Appl. Phys. Lett. **62**, 1047 (1993).
11. B. H. Kolner, Appl. Phys. Lett. **52**, 1122 (1988).
12. G. P. Agrawal, *Nonlinear Fiber Optics*, 5th ed. (Elsevier, Amsterdam, 2013).
13. C. Dorrer and J. Bromage, Opt. Lett. **35** 1353 (2010).
14. High Q Laser Production GmbH, model femtoTRAIN IC-1053-400 fsYb, see <http://www.spectra-physics.com/products/ultrafast-lasers/femtotrain> (25 February 2015).
15. EOSpace, Inc., Redmond, WA 98052; see <http://www.eospace.com> (25 February 2015).
16. I. Kang, C. Dorrer, and F. Quochi, Opt. Lett. **28**, 2264 (2003).
17. Yokogawa Electric Corporation, Optical Spectrum Analyzer, Model AQ6317b, see <http://tmi.yokogawa.com/discontinued-products/ando/ando/810804100-aq6317b-optical-spectrum-analyzer/> (26 February 2015).